Progress In Electromagnetics Research, Vol. 139, 611–626, 2013

A NEW CONICAL-TRAJECTORY POLAR FORMAT ALGORITHM FOR SPOTLIGHT BISTATIC SAR

Yan Wang, Jingwen Li, Bing Sun*, Jie Chen, and Huaping Xu

School of Electronic and Information Engineering, Beihang University, Beijing, China

Abstract—The Polar Format Algorithm (PFA) is suitable for spotlight synthetic aperture radar (SAR) image focusing either in monostatic or bistatic cases. The classic linear-trajectory PFA complete data correction in wavenumber domain, converting data from the polar format to the rectangular format. However, the two-dimension processing (either using interpolation or chirp-z transform) introduces heavy computational load, which limits its real-time applications. This study presents a conical-trajectory PFA for bistatic SAR, in which the transmitter and receiver are designed to fly on conical surfaces, to simplify image formation procedures via eliminating the necessity of range processing. Moreover, the conical-trajectory PFA provides a space-invariant range resolution to simplify the SAR image comprehension. A spotlight forward-looking bistatic missile guidance application was simulated for the algorithm validation and performance analysis.

1. INTRODUCTION

Spotlight synthetic aperture radar (SAR) is a remote sensing instrument providing the opportunity to collect data over a wide azimuth angular interval with the potential for extremely high azimuth resolution [1–3]. As a standard all-weather reconnaissance tool, SAR plays important roles in geological disaster monitoring [4, 5], biological environment estimation [6, 7] and ground moving target identification [8, 9]. Since firstly invented as a spotlight SAR

Received 19 March 2013, Accepted 6 May 2013, Scheduled 13 May 2013

* Corresponding author: Bing Sun (sun8839@gmail.com).

algorithm in 1969, Polar Format Algorithm (PFA) has been attracting focuses for its simple processing steps and low requirement for A/D sample rate. PFA can be employed for spotlight mode either in monostatic or bistatic geometry [1, 10–13]. However, in the classic lineartrajectory PFA, the range processing (either sinc-interpolation or chirp-z transformation) introduces heavy computational load, which limits the image formation speed and its real-time applications. Moreover, in bistatic cases the two-dimension resolution varies with positions of the transmitter and receiver, which complicates the SAR image comprehension.

This study presents a new conical-trajectory PFA for the bistatic SAR to simplify the image formation procedure by eliminating the range processing. When the transmitter and receiver fly on each conical surface with a same vertex at the center reference point (CRP), data can be collected directly in the trapezoidal format. By converting part of computation of image processor to the navigation and location system, image formation speed can be obviously accelerated. In addition, the conical-trajectories PFA has a further advantage of realizing a space-independent synthetic range resolution. A potential spotlight forward-looking bistatic missile guidance application was used for analysis. While a passive receiver of relatively low cost may be boarded on the missile to receive the reflected data, a higher cost transmitter staying at a safe standoff distance can be precisely controlled to move along conical trajectories [13]. If the bistatic SAR was used for guiding precise attacking task, the passive receiver could be designed to follow a linearly or spirally path towards the target on the required conical surfaces. Contrary to our preliminary research results in [14], the bistatic conical-trajectory PFA was further developed in this paper with a much more detailed mathematical derivations of imaging process, feasible trajectories for both the transmitter and receiver, much stricter resolution analysis as well as richer simulation results.

This paper is organized as follows. In Section 2, spotlight bistatic signal mode SAR is described. The principle of the conical-trajectory algorithm is derived in Section 3. Bistatic resolution performance is analyzed in Section 4. Section 5 briefly introduces several feasible applications following the conical-trajectory principle. Section 6 validates the proposed conical-trajectory PFA via computer simulation. Lastly, Section 7 provides the summary and suggestions for the future work.

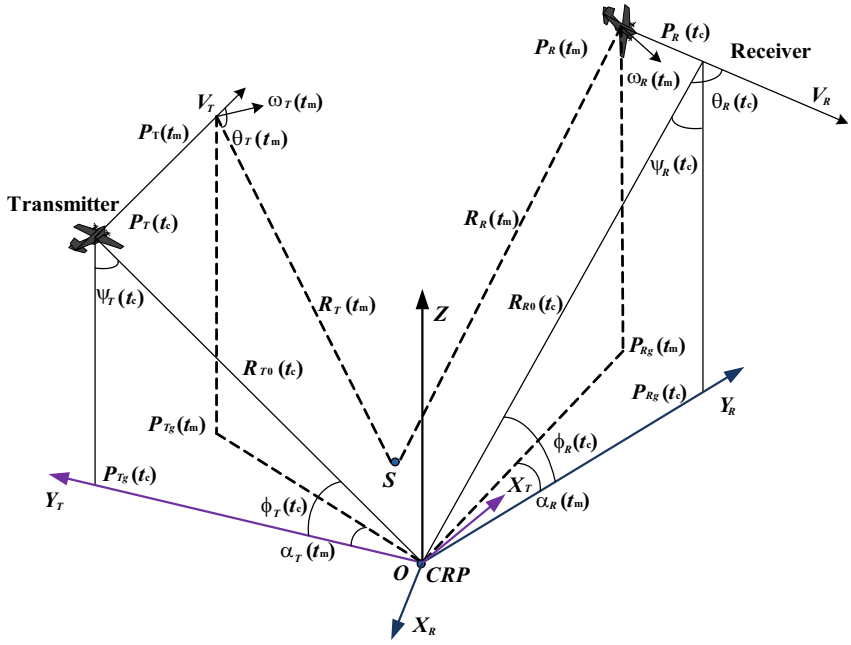

Figure 1. Spotlight bistatic SAR geometry.

2. SIGNAL MODE OF SPOTLIGHT BISTATIC SAR

Figure 1 shows a general bistatic SAR geometry, in which two Cartesian coordinates system are built due to the transmitter and receiver positions. While the two coordinates share the same original point (CRP) and Z-axis, the Y-axis of the transmitter coordinate is Y_T and the receiver coordinate is Y_R. X_T and X_R are formed by the right hand principle P_T and P_R are assumed to be instant positions of the transmitter and receiver. P_{Tg} and P_{Rg} are projections of P_T and P_R in the ground plane. t_m is the slow (azimuth) sampling time and t_c is the central synthetic aperture time. Y_T follows direction of $\mathbf{OP}_{Tg}(t_c)$ and Y_R follows direction of $\mathbf{OP}_{Rg}(t_c)$. $\mathbf{R}_{T0}$ and $\mathbf{R}_{R0}$ are vectors from the CRP to P_T and P_R. Assuming S depicts a certain scatterer in the illuminated area, $\mathbf{R}_T$ and $\mathbf{R}_R$ depict vectors from S to P_T and P_R, respectively. ψ_T and ψ_R are instant incidence angles of the transmitter and receiver. α_T is the angle between $\mathbf{OP}_{Tg}$ and Y_T. α_R is the angle formed by $\mathbf{OP}_{Rg}$ and Y_R.

A linear frequency modulated (LFM) signal is assumed for area

illumination. The echoed signal yields

$$S_r(\tau, t_m) = \text{rect}\left[\frac{\tau - R(t_m)/c}{T_p}\right] \text{rect}\left[\frac{t - t_c}{T_{syn}}\right] \exp\left\{j2\pi\left[f_c\left(t - \frac{R(t_m)}{c}\right) + \frac{1}{2}\gamma\left(\tau - \frac{R(t_m)}{c}\right)^2\right]\right\} \quad (1)$$

where c is the light speed. τ is the fast (range) time. T_p is the pulse duration. T_{syn} is the synthetic aperture time. f_c and γ depict the carrier frequency and chirp rate of LFM signal, respectively. $R(t_m) = R_T(t_m) + R_R(t_m)$.

PFA employs the dechirped signal for image formation. By multiplying a conjugate reference signal, the signal yields

$$S_{if}(\tau, t_m) = \exp\left\{-j\frac{2\pi}{c}\left[f_c + \gamma\left(\tau - \frac{R_{ref}(t_m)}{c}\right)\right] R_\Delta(t_m)\right\} \exp\left\{j\frac{\pi\gamma\left(R(t_m) - R_{ref}(t_m)\right)^2}{c^2}\right\}. \quad (2)$$

After compensating the residual video phase (RVP) using a frequency-domain matched filter [1], the signal yields

$$S_{if}(\tau, t_m) = \exp\left\{-jK(\tau, t_m)\left(R(t_m) - R_{ref}(t_m)\right)\right\} \quad (3)$$

where the wavenumber $K(\tau, t_m)$ is defined as

$$K(\tau, t_m) = \frac{2\pi}{c}\left(f_c + \gamma\left(\tau - \frac{R_{ref}(t_m)}{c}\right)\right). \quad (4)$$

To agree with the real discrete time SAR system, signal should be digitalized as

$$S_{if}(i, m) = \exp\left\{-jK(i)\left(R_T(m) - R_{T0}(m)\right)\right\} \exp\left\{-jK(i)\left(R_R(m) - R_{R0}(m)\right)\right\} \quad (5)$$

$$K(i) = \frac{2\pi}{c}\left(f_c + i\frac{\gamma}{N_r F_s}\right) \quad (6)$$

where N_r denotes the total sample number along the range direction. i and m denote the range and azimuth sample serial numbers, respectively. F_s is the range sample rate. R_{T0} and R_{R0} indicate the distances from the scene center to the transmitter and receiver, respectively.

Observe the geometry shown in Figure 2. The Y_S-axis follows the projection of synthetic range resolution in the ground plane. The X_S-axis is determined by the right hand principle. Ω_{T0} is the angle

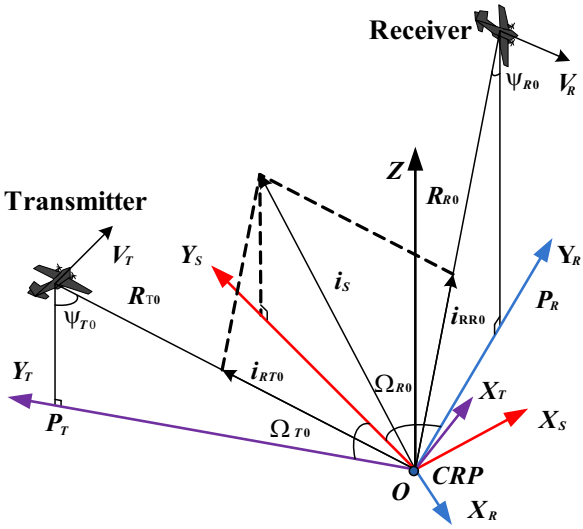

Figure 2. Geometry for imaging analysis.

between the Y_T and Y_S. Ω_{R0} is the angle between the Y_R and Y_S. A scatterer is assumed to have a $(x_T, y_T, 0)$ coordinate in X_TY_TZ plane, a $(x_R, y_R, 0)$ coordinate in X_RY_RZ plane and a $(x_S, y_S, 0)$ coordinate in X_SY_SZ plane. According to the definition of the three coordinate systems, we have

$$\begin{cases} x_T = x_S \cos\Omega_{T0} + y_S \sin\Omega_{T0} \\ y_T = -x_S \sin\Omega_{T0} + y_S \cos\Omega_{T0} \end{cases}. \tag{7}$$

$$\begin{cases} x_R = x_S \cos\Omega_{R0} - y_S \sin\Omega_{R0} \\ y_R = x_S \sin\Omega_{R0} + y_S \cos\Omega_{R0} \end{cases}. \tag{8}$$

Overlooking the wavefront curve, phase of $S_{if}(i,m)$ in (5) can be expressed in wavenumber domain as

$$\begin{aligned} \varphi(i,m) \;=\; & K(i)\sin\psi_T(m)\cos\alpha_T(m)\left(y_T + \tan\alpha_T(m)x_T\right) \\ & + K(i)\sin\psi_R(m)\cos\alpha_R(m)\left(y_R + \tan\alpha_R(m)x_R\right). \end{aligned} \tag{9}$$

Substituting (7) and (8) into (9), signal $\varphi(i,m)$ yields

$$\varphi(i,m) = K_{SY}(i,m)y_S + K_{SX}(i,m)x_S \tag{10}$$

where K_{SX} and K_{SY} are wavenumbers along the direction of X_S and Y_S, respectively, which yield

$$\begin{aligned} K_{SY}(i,m) &= K(i)\left(\cos\left(\alpha_T(m)-\Omega_{T0}\right)\sin\psi_T(m)\right. \\ &\quad \left.+\cos\left(\alpha_R(m)+\Omega_{R0}\right)\sin\psi_R(m)\right). \end{aligned} \tag{11}$$

$$\begin{aligned} K_{SX}(i,m) &= K(i)\left(\sin\left(\alpha_T(m)-\Omega_{T0}\right)\sin\psi_T(m)\right. \\ &\quad \left.+\sin\left(\alpha_R(m)+\Omega_{R0}\right)\sin\psi_R(m)\right). \end{aligned} \tag{12}$$

3. BISTATIC CONICAL-TRAJECTORY PFA

In the classic linear-trajectory PFA, data should be converted from the polar format to the trapezoidal format via the range processing. In this case, the K_{SY} will be scaled to have uniformly distributed sample intervals. However, either the sinc-interpolation or the chirp-z transform employed to conduct the range correction will result in heavy computational load, especially for high resolution and large swath imaging cases [1, 15]. This study proposes a conical-trajectory PFA to accelerate the imaging speed by eliminating the necessity of the range processing. The strategy is to design special flight trajectories for the transmitter and receiver to realize a space independent K_{SY}. In this case, the received data can be directly stored in the trapezoidal format and the range processing procedure can be wiped off. To simplify analysis, we define

$$F_{SY}(m) = F_{SYT}(m) + F_{SYR}(m) \tag{13}$$

where

$$F_{SYT}(m) = \cos\left(\alpha_T(m)-\Omega_{T0}\right)\sin\psi_T(m). \tag{14}$$

$$F_{SYR}(m) = \cos\left(\alpha_R(m)+\Omega_{R0}\right)\sin\psi_R(m). \tag{15}$$

To keep K_{SY} in (13) independent of azimuth indicator m, a feasible method is to realize time-invariant F_{SYT} and F_{SYR}. To clarify the requirement for flight trajectories of the transmitter and receiver, F_{SYT} is taken for analysis, which is similar for F_{SYR}.

Based on geometry in Figure 2, F_{SYT} yields

$$F_{SYT}(m) = \cos\left(\alpha_T(m)-\Omega_{T0}\right)\sin\psi_T(m) = \cos(\phi_T(m)). \tag{16}$$

Equation (16) implies the condition for F_{SYT} being unchanged: ϕ_T should be kept as a constant during the synthetic aperture time. In this case, trajectory of the transmitter should be on a conical surface, of which the vertex locates at the *CRP*, the cone angle is ϕ_T and the cone axis follows the direction of Y_S, as depicted in Figure 3.

For the receiver, F_{SYR} yields

$$F_{SYR}(m) = \cos\left(\alpha_R(m)+\Omega_{R0}\right)\sin\psi_R(m) = \cos(\phi_R(m)). \tag{17}$$

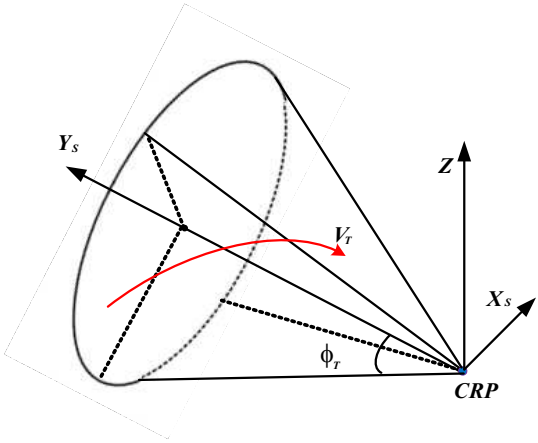

Figure 3. Schematic figure for conical trajectory.

As ϕ_R should also be constant to make F_{SYR} unchanged, the flight trajectory of receiver should also be on a conical surface. While the vertex and the cone axis are the same with the transmitter, the cone angle is ϕ_R. Then $K_{SY}(i,m)$ can be scaled as $K_{SY}(i,0)$, which can be substituted into (10) as

$$\varphi(i,m) = K_{SY}(i,0)\left(y_S + \frac{K_{SX}(i,m)}{K_{SY0}(i,0)}x_S\right). \tag{18}$$

As shown in Figure 3, data along the cross-range direction (K_{SX}) is not uniformly distributed. To ideally focus SAR images, the azimuth intervals should be uniformly scaled for each range gate. Then a cross-range interpolation can be used to convert the data from the trapezoidal format to the rectangular format as depicted in (19).

$$m' = K_{SX}(i,m)\frac{N_a}{K_{SX}\left(-\frac{N_r}{2},\frac{N_a}{2}\right) - K_{SX}\left(-\frac{N_r}{2},-\frac{N_a}{2}\right)} \tag{19}$$

where N_a denotes the total azimuth sample number. Substituting (19) into (18), we have

$$\varphi(i,m') = b_1 y_S + b_2 y_S i + b_3 x_S m' \tag{20}$$

where

$$\begin{cases} b_1 = \dfrac{2\pi f_c F_{SY}(0)}{c} \\ b_2 = \dfrac{2\pi\gamma F_{SY}(0)}{cN_r F_s} \\ b_3 = \dfrac{K_{SX}\left(-\frac{N_r}{2},\frac{N_a}{2}\right) - K_{SX}\left(-\frac{N_r}{2},-\frac{N_a}{2}\right)}{N_a} \end{cases} \tag{21}$$

A followed two cascade one-dimension IFFTs will complete image focusing along the range and azimuth direction. The system impulse response function (IRF) yields

$$I(n,k) = A\exp\{jb_1y_S\}\sum_{i=0}^{N_r-1}\exp\left\{j\left(b_2y_S+\frac{2\pi n}{N_r}\right)i\right\} \sum_{m'=0}^{N_a-1}\exp\left\{j\left(b_3x_S+\frac{2\pi k}{N_a}\right)m'\right\} \quad (22)$$

where A represents the signal amplitude. The flowchart of the conical-trajectory PFA is shown in Figure 4.

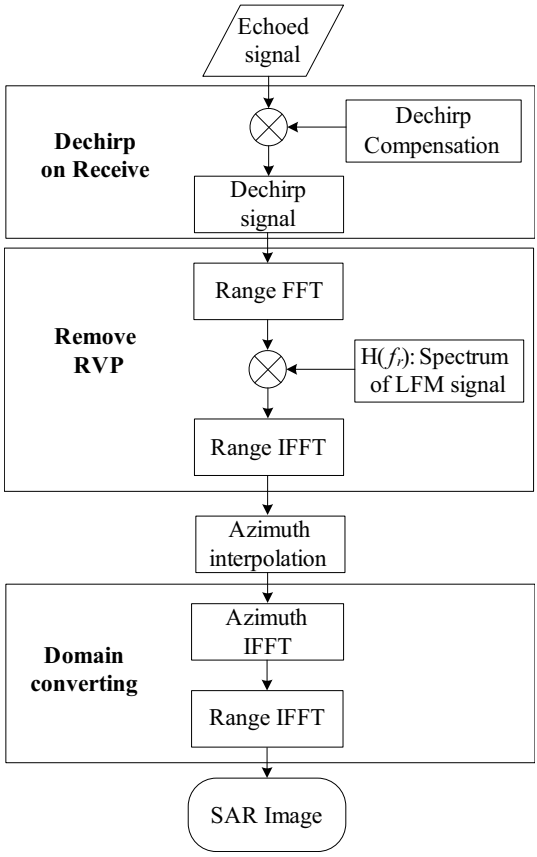

Figure 4. Flowchart of the conical-trajectory PFA.

4. RESOLUTION ANALYSIS

The space-variant feature of resolution tends to be more serious in bistatic SAR case than that in the monostatic case. By adopting the gradient analyzing method [16], the conical-trajectory PFA contributes to an invariant range resolution. In this case, SAR image comprehension and the follow-up image processing will be simplified. As the space variety of azimuth resolution is inevitably, the azimuth resolution at the central synthetic aperture time is often employed for approximation.

4.1. Range Resolution

B is assumed to be the signal bandwidth and $\mathbf{G}_R$ is assumed to be the gradient of slant range along a certain direction, the range resolution along the same direction yields

$$\rho_R = \frac{c}{B\left|\mathbf{G}_R\right|} \tag{23}$$

In bistatic SAR system, the range resolution can be defined to be

$$\rho_r = \frac{c}{B\left|\mathbf{g}_R\right|^2}\mathbf{g}_R \tag{24}$$

where $\mathbf{g}_R$ depicts the gradient of R_{ref} in the X_sOY_s plane, which yields

$$\mathbf{g}_R = \left(\cos\Omega_T \sin\psi_T + \cos\Omega_R \sin\psi_R\right)\mathbf{i}_{YS} \tag{25}$$

where the i_{YS} denotes the unit vector along the Y_s-axis in Figure 2. As introduced in Section 2, when the transmitter and receiver fly on the required conical surfaces, $(\cos\Omega_T \sin\psi_T)$ and $(\cos\Omega_R \sin\psi_R)$ are guaranteed as both constants, so as to $|\mathbf{g}_R|$. In this case, a space-independent range resolution for the bistatic SAR system can be achieved.

4.2. Azimuth Resolution

The Doppler frequency resolution of bistatic SAR can be defined as

$$\nabla f_a = \frac{1}{\lambda}\left(\omega_T + \omega_R\right) \tag{26}$$

where ω_T and ω_R depict the angular speed vectors of the transmitter and receiver as shown in Figure 1, respectively. f_a depicts the Doppler frequency of the echoed signal

$$f_a = \frac{1}{2\pi}\frac{d\varphi(t)}{dt} = -\frac{1}{\lambda}\left(V_T\cos\theta_T + V_R\cos\theta_T\right). \tag{27}$$

To discriminate the adjacent scatterers the transient Doppler frequency difference of two adjacent scatterers should be larger than $1/T_{syn}$ which denotes the space Doppler resolution. As a result, the bistatic azimuth resolution ρ_a in the X_sOY_s (ground) plane yields

$$\rho_a = \frac{\lambda}{T_{syn} \left| \mathbf{Z}_{xy} \left(\omega_T + \omega_R \right) \right|} \tag{28}$$

where $\boldsymbol{Z}_{xy}$ is the matrix projecting data from three-dimension space to two-dimension ground plane.

Eqation (28) implies a variant azimuth resolution of bistatic SAR given the space-dependent ω_T and ω_R. When ω_T and ω_R share the same direction with the maximum norms of projection of the ground plane, the azimuth resolution achieves its maximum value. The ρ_a at the central aperture time is often viewed approximately as the bistatic SAR azimuth resolution.

5. FEASIBLE BISTATIC GEOMETRY AND APPLICATION

One feasible application of the conical-trajectory PFA comes to the real-time military monitory and precise attack. When the transmitter staying at safe distance illuminates the area of interest, the passive receiver boarded on a lower cost attacking unit can penetrate the hostile areas and destroy targets. Several feasible conical trajectories of the transmitter and receiver are briefly introduced below.

5.1. Transmitter

In this section we focus on two conical modes: the fixed altitude mode and the linear ground-projection mode. The transmitter is assumed

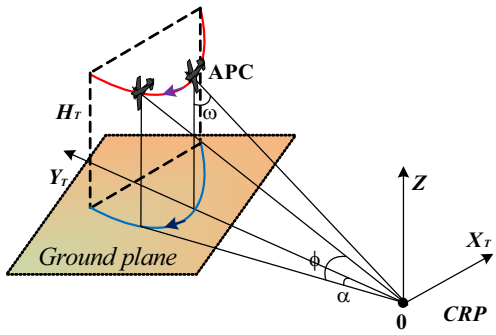

Figure 5. Hyperbola trajectory for the fixed altitude mode.

to fly in a certain fixed planar plane denoted as L_T. The transmitter trajectory is determined by the intersection line formed by L_T and the conical surface. If the transmitter moves with a fixed altitude, L_T is parallel with the ground plane, which leads to a hyperbola trajectory as shown in Figure 5. If the velocity projection of sensor on the ground plane follows a fixed direction, the flight trajectory should be part of an ellipse with one focus overlapping with the intersection point of the cone axis and L_T. Figure 6 depicts the elliptical mode.

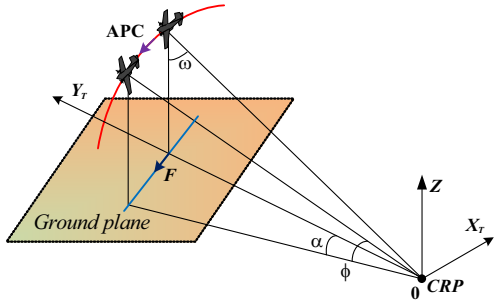

Figure 6. Ellipse trajectory for the linear ground-projection mode.

5.2. Receiver

In this section a bistatic forward-looking bistatic geometry is adopted for analysis. It is found when the receiver flies a linear trajectory, which satisfies the very conical requirement as shown in Figure 7(a). However, such geometry implies a simple attacking path that would be easy to predict and intercept. To increase the surviving rate, the

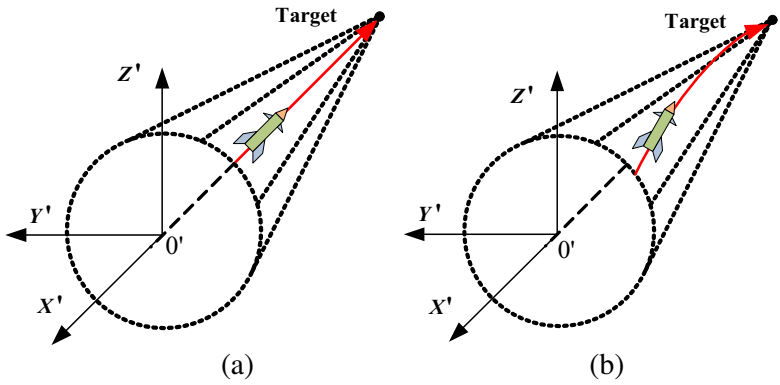

Figure 7. Linear and spiral trajectory for the receiver.

receiver can fly flexibly along any spiral curves on the conical surface towards target as shown in Figure 7(b). In Figure 7, $X'O'Y'$ represents the ground plane.

6. SIMULATION AND ANALYSIS

In this section, a spotlight bistatic forward-looking SAR system (displayed in Figure 8) is employed to validate the conical-trajectory PFA via multi-scatterer computer simulations. The receiver is assumed to fly linearly towards the illuminating center and the transmitter is assumed keep a fixed altitude mode. A Ku-Band LFM signal is

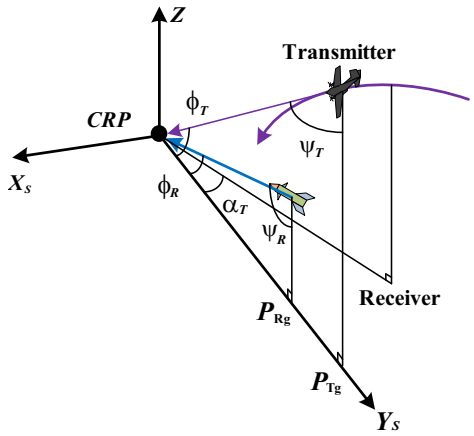

Figure 8. The bistatic forward-looking geometry used for simulation.

Table 1. Simulation parameters.

Parameter	Value
Wavelength	0.025 m
Pulse duration	3 μs
Bandwidth	180 MHz
Transmitter velocity	300 m/s
Receiver velocity	500 m/s
Sampling frequency	400 MHz
Transmitter center range	10 km
Receiver center range	5.8 km
Scene radius	100 m

assumed for transmitting and the bistatic SAR has a 1 m resolution along both the range and azimuth directions. Simulation parameters are listed in Table 1. Scatterers are assumed to have the same backscatter coefficient and distributed within a circle of 100 m radius.

Table 2. Image quality inspection for point A.

		Measured value	Theoretical value
Range	PSLR (dB)	−14.65	−13.26
	ISLR(dB)	−12.73	−9.80
	ρ_r(m)	0.95	1.00
Azimuth	PSLR(dB)	−14.63	−13.26
	ISLR(dB)	−11.03	−9.80
	ρ_a (m)	1.03	1.00

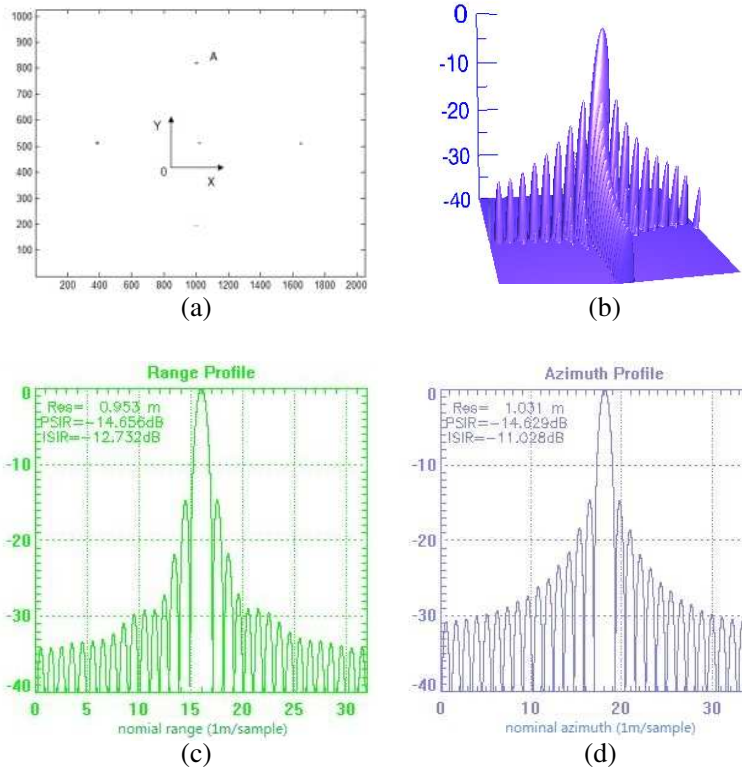

Figure 9. Image result and quality inspection.

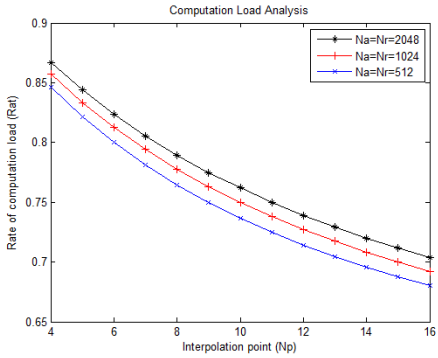

Figure 10. Schematic figure for computational load.

The simulated SAR image focused by the conical-trajectory PFA is shown in Figure 9(a). The two-dimension IRF of points A (shown in Figure 9(b) is used to inspect algorithm performance Figure 9(c) and Figure 9(d) display the range and azimuth profiles, respectively. Peak side lobe ratio (PSLR) integral side lobe ratio (ISLR) and resolution performance of point A are given in Table 2. Since the measured values correspond well with the theoretical ones of ideal sinc(·) function, the validity of the conical-trajectory algorithm is confirmed.

Compared with the linear-trajectory PFA, the conical-trajectory PFA largely decreases computational load. Figure 10 displays the computational load that is saved by the conical-trajectory PFA. The X-label (N_p) depicts the interpolation kernel length and the Y-label presents the rate of computational load (Rat) of the conical-trajectory PFA to the linear-trajectory PFA. N_a and N_r are assumed to share the same values for the analysis.

Figure 10 indicates that by increasing length of interpolation kernel, the computational load introduced by the conical-trajectory PFA tends to get smaller than that caused by linear trajectory PFA. Besides, sampling numbers along the range and azimuth also affect the computational efficiency. By decreasing N_a and N_r, the rate of saved computational load will increase. Choice should be balanced considering the required sample numbers and the limited length of interpolation kernel to achieve an optimized real-time system performance.

7. CONCLUSION

In this study, a conical-trajectory PFA for the spotlight bistatic SAR was presented to improve the system real-time performance

and to realize an invariant range resolution. By designing conical trajectories for the transmitter and receiver, the range processing, which originally converts data from the polar format to the trapezoidal format in the classic linear-trajectory PFA, can be avoided. In this case, the computational load was obviously decreased for benefit of the simplification of the imaging procedure. System resolution was analyzed in detail and the derivation indicated that the conical-trajectory PFA can realize an invariant range resolution. In occasion of a missile guidance task, several conical trajectories for the transmitter and receiver are briefly introduced. A Multi-scatterer simulation employing the spotlight bistatic forward-looking geometry validated the presented approach.

Future researches may focus on the combination of the conical-trajectory PFA with overlap subaperture algorithm (OSA) to enlarge the valid image swath. The extensional usages of the conical-trajectory PFA for space-borne tasks are also worth studying

ACKNOWLEDGMENT

This work was supported by the Innovation Foundation of BUAA for Ph.D. Graduates.

REFERENCES

1. Carrara, W. G., R. S. Goodman, and R. M. Majewski, *Spotlight Synthetic Aperture Radar*, Artech House, MA, USA, 1995.
2. Lou, J., T. Jin, and Z. Zhou, "Feature extraction for landmine detection in UWB SAR via SWD and isomap," *Progress In Electromagnetics Research*, Vol. 138, 157–171, 2013.
3. Yang, W., J. Chen, H. Zeng, J. Zhou, P. Wang, and C.-S. Li, "A novel three-step image formation scheme for unified focusing on spaceborne SAR data," *Progress In Electromagnetics Research*, Vol. 137, 621–642, 2013.
4. Raucoules, D. and M. de Michele, "Assessing ionoshperic influence on L-band SAR data implications on coseismic displacement measurements of the 2008 Sichuan earthquake," *IEEE Trans. Geosci. Remote Sens.*, Vol. 7, No. 2, 286–290, Apr. 2010.
5. Dellepiane, S. G. and E. Angiati, "A new method for cross-normalization and multitemporal visualization of SAR images for the detection of flooded areas," *IEEE Trans. Geosci. Remote Sens.*, Vol. 50, No. 7, 2765–2779, Jul. 2012.

6. Srivastava, H. S., P. Patel, Y. Sharma, and R. R. Navalgund, "Large-area soil moisture estimation using multi-incidence-angle RADARSAT-1 SAR data," *IEEE Trans. Geosci. Remote Sens.*, Vol. 47, No. 8, 2528–2535, Aug. 2009.
7. Singh, D. and A. Kathpalia, "An efficient modeling with GA approach to retrieve soil texture, moisture and roughness from ERS-2 SAR data," *Progress In Electromagnetics Research*, Vol. 77, 121–136, 2007.
8. Tian, B., D.-Y. Zhu, and Z.-D. Zhu, "A novel moving target detection approach for dual-channel SAR system," *Progress In Electromagnetics Research*, Vol. 115, 191–206, 2011.
9. Mao, X., D.-Y. Zhu, L. Ding, and Z.-D. Zhu, "Comparative study of RMA and PFA on their responses to moving target," *Progress In Electromagnetics Research*, Vol. 110, 103–124, 2010.
10. Xu, H., J. Gao, and J. Li, "A variable prf imaging method for high squint diving SAR," *Progress In Electromagnetics Research*, Vol. 135, 215–229, 2013.
11. Liu, Q., W. Hong, W. Tan, Y. Lin, Y. Wang, and Y. Wu, "An improved polar format algorithm with performance analysis for geosynchronous circular SAR 2D imaging," *Progress In Electromagnetics Research*, Vol. 119, 155–170, 2011.
12. Wang, Y., Y. J. Li, J. Chen, H. Xu, and B. Sun, "A novel non-interpolation polar format algorithm using non-lineal flight trajectories and auto-adaptive PRF technique," *Progress In Electromagnetics Research*, Vol. 122, 155–173, 2012.
13. Rigling, B. D., "Polar format algorithm for bistatic SAR," *IEEE Trans. Aerosp. Electron. Syst.*, Vol. 40, No. 4, 1147–1159, Oct. 2004.
14. Wang, Y., J. W. Li, J. Chen, H. P. Xu, and B. Sun, "A new trajectory-based polar format algorithm for bistatic SAR," *IEEE IGARSS*, 319–322, 2012.
15. Tang, Y., M.-D. Xing, and Z. Bao, "The polar format imaging algorithm based on double chirp-z transforms," *IEEE Geosci. Remote Sens. Lett.*, Vol. 5, No. 4, 610–614, Oct. 2008.
16. Moccia, A. and A. Renga, "Spatial resolution of bistatic synthetic aperture radar: Impact of acquisition geometry on imaging performance," *IEEE Trans. Geosci. Remote Sens.*, Vol. 49, No. 10, 3487–3503, Oct. 2011.